Behavior of Integrated Crosstie Trackwork System

Colin MacDougall[1]; T. Ivan Campbell[2]; David Swanson[3]; Yail J. Kim[4]; and Harry R. Skoblenick[5]

Abstract: Light rail systems are an important transportation mode in urban centers. An advanced rail transit system has been developed that utilizes linear induction motors (LIM) for propulsion and braking of the vehicles. Due to the tight motor-to-rail air gap tolerances required for the efficient operation of the LIM system, the trackwork requires special consideration. An innovative crosstie trackwork system has been developed to address competing requirements for high stiffness to ensure efficient operation of the LIM, and low track stiffness for acceptable ride quality. The crosstie incorporates a hollow structural steel section welded at each end to formed steel base plates which are supported by elastomeric pads. The crosstie supports steel running rails. This paper describes a finite-element model developed to predict the response of a crosstie to loads that simulate the passage of a steel wheeled transit vehicle. The model uses tetrahedral elements for the hollow structural steel section and the base plates. The elastomeric pads are modeled using elastic foundation elements. The model predicts stresses and deflections in the crosstie. An experimental program that was carried out on the crosstie to investigate its fatigue performance and to obtain data to verify the finite-element model is also described. The model conservatively predicts crosstie deflections and stresses. The hot spot stress approach is used to provide a conservative fatigue life prediction of the crosstie.

DOI: 10.1061/(ASCE)0733-9445(2008)134:2(329)

CE Database subject headings: Fatigue life; Finite element method; Structural behavior; Railroad ties.

Introduction

Light rail systems are an important transportation mode in many urban centers (Fatemi et al. 1996). Fig. 1(a) shows an advanced rapid transit (ART) vehicle and Fig. 1(b) shows the details of one of the bogies. The vehicle uses linear induction motors (LIM) mounted beneath the vehicle for braking and propulsion. The LIM primary on the vehicle consists of electromagnets that produce eddy currents in the LIM reaction rail, which is a steel back-iron structure capped by an aluminum top cap and mounted on the centerline of the track. Fig. 1(c) shows the trackwork. There is a 10 mm air gap between the LIM primary and the LIM reaction rail. During vehicle operation, the electromagnetic forces between the LIM primary and the LIM reaction rail pull up on the rail and tend to reduce the air gap. In order for the system to operate efficiently, this air gap cannot be reduced by more than 1–2 mm. An innovative system that integrates the LIM reaction rail and the running rails through a steel crosstie supported by elastomeric pads has been proposed.

Fig. 2 provides details of the crosstie. A steel hollow structural section (HSS) is welded to formed steel base plates which are in turn supported on elastomeric pads. The base plates are stiffened by welded gussets in the corners. Anchor bolts connect the crosstie to the concrete guideway. The high stiffness of the crosstie structure ensures the tight tolerances required in the height of the air gap between the track mounted LIM secondary rail and the vehicle mounted LIM primary are maintained, while the low stiffness of the elastomeric pads ensures an acceptable ride quality.

There are a number of performance criteria that the system

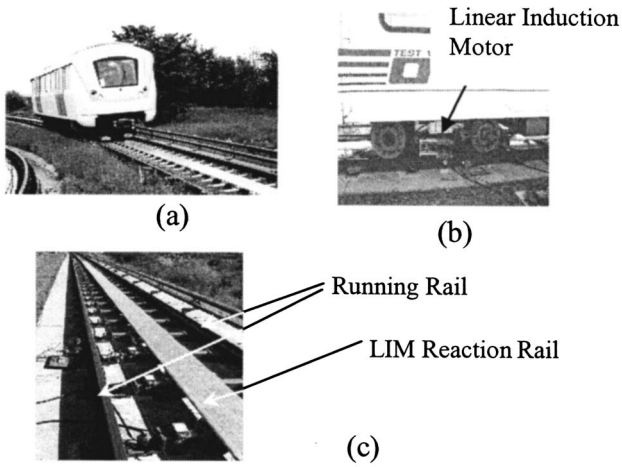

Fig. 1. Advanced rapid transit system: (a) vehicle; (b) bogie; (c) trackwork

[1]Assistant Professor, Dept. of Civil Engineering, Queen's Univ., Kingston, ON, Canada K7L 3N6 (corresponding author). E-mail: colin@civil.queensu.ca

[2]Emeritus Professor, Dept. of Civil Engineering, Queen's Univ., Kingston, ON, Canada K7L 3N6.

[3]Design Engineer, Delcan Associates, Toronto, ON, Canada M3C 1K1.

[4]Assistant Professor, Dept. of Civil Engineering, North Dakota State Univ., Fargo, ND 58105. E-mail: jimmy.kim@ndsu.edu

[5]Project Engineer, Fixed Facilities, Bombardier Transportation, Kingston, ON, Canada K7M 6R2.

Note. Associate Editor: M. Asghar Bhatti. Discussion open until July 1, 2008. Separate discussions must be submitted for individual papers. To extend the closing date by one month, a written request must be filed with the ASCE Managing Editor. The manuscript for this paper was submitted for review and possible publication on November 10, 2005; approved on September 22, 2006. This paper is part of the ***Journal of Structural Engineering***, Vol. 134, No. 2, February 1, 2008. ©ASCE, ISSN 0733-9445/2008/2-329–336/$25.00.

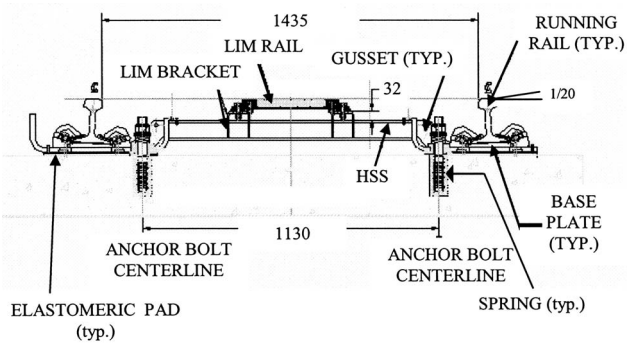

Fig. 2. Details of crosstie

must satisfy. It is important that maximum stresses do not exceed the yield strength of the steel to ensure that permanent deformation or material failure do not occur under service loads. It is also critical that the relative deflection between the running rail and the top of the LIM does not exceed 2.0 mm under maximum loads. This relative deflection is a measure of a change in the LIM air gap. In addition, welded steel structures are susceptible to fatigue cracking when subjected to millions of cyclic loads. Critical stresses in the crosstie when subjected to service loads must be assessed to ensure that fatigue limit states are not exceeded.

In addition to these design criteria, the cost of the crosstie and its installation and maintenance must be as economic as possible. The reduction in these costs is significant, because in a typical installation, crossties are spaced every 1 m. The reduction in cost of even a few dollars per crosstie therefore results in a significant savings for a typical installation. Several designs of the crosstie have been proposed (Fatemi 1993). Because the fabrication and testing of a given crosstie design are costly and time-consuming, finite-element modeling of the crosstie is proposed so that the impact of design changes on the structural response of the crosstie can be quickly and economically assessed.

Previous work on timber, concrete, and steel crossties has focused on understanding the forces applied to the crosstie through the trackwork (Kerr and Zarembski 1986; Tarran 1987) but there has been little attention paid to the stresses the crosstie itself must resist. This becomes especially relevant as the design becomes more sophisticated. The present paper is focused on the structural response of the crosstie shown in Fig. 2. The finite-element model for predicting stresses and deflections of the crosstie is described. Laboratory testing of the crosstie is carried out to verify the

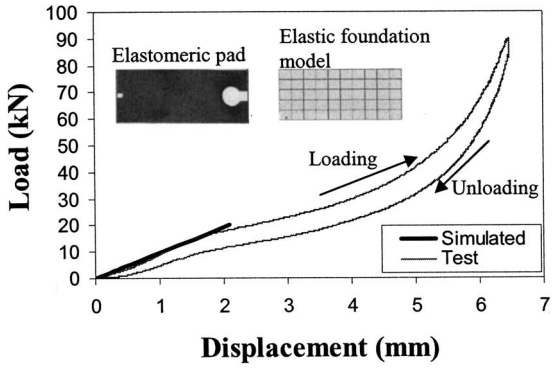

Fig. 3. Load-displacement response of elastomeric pad in compression

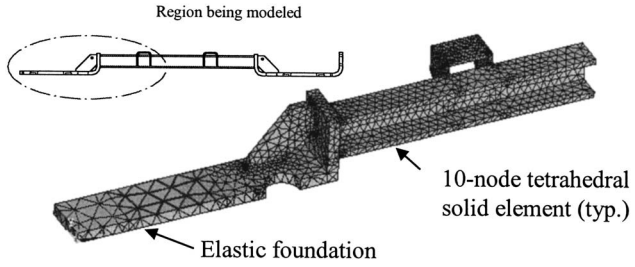

Fig. 4. Meshing for crosstie FEA model

model predictions and to ensure that fatigue cracking of the crosstie does not occur after the application of 3×10^6 cycles of service loading. The finite-element model results are also used to estimate the fatigue life of the crosstie.

Finite-Element Modeling

The commercial finite-element analysis (FEA) software package ANSYS (ANSYS 2003) was used to develop a model of the crosstie. Initially, a linear FEA model using shell elements was developed to predict the behavior of the crosstie and compared to experimental data (MacDougall et al. 2003). The model showed good agreement with measured stress; however, the model underestimated the displacement of the crosstie.

Fig. 3 shows the load versus deformation response of the polyurethane elastomeric pad. The pad is approximately 170 mm wide, 454 mm long, and 12 mm thick. The experimental results were obtained by uniformly compressing a pad between two steel loading platens. The displacement given in Fig. 3 is the average of values measured at three locations on the pad. The response is nonlinear. Upon loading, the pad's stiffness increases with load until the load is about 17 kN. The stiffness of the pad then decreases with increasing load up to about 35 kN, subsequent to which the stiffness again increases with load. Upon unloading, the pad exhibits hysteresis.

The modeling of nonlinear materials can be complex in FEA. However, up to about 2 mm pad deflection, the response can reasonably be modeled as linear. As will be described in the experimental results, the deflections of the pad under maximum service loads are about 2 mm. Therefore, the pad was modeled using the elastic foundation element in ANSYS.

Fig. 3 shows an elevation view of the elastomeric pad and the meshed elastic foundation model. Note that the elastomeric pad has small cutouts to accommodate the anchor bolts, however these amount to less than 2.5% of the area and so were not included in the model. The stiffness of the elastic foundation elements was varied until the simulated load deflection response of

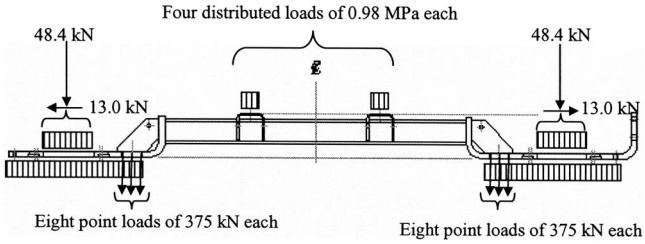

Fig. 5. Free-body diagram of crosstie

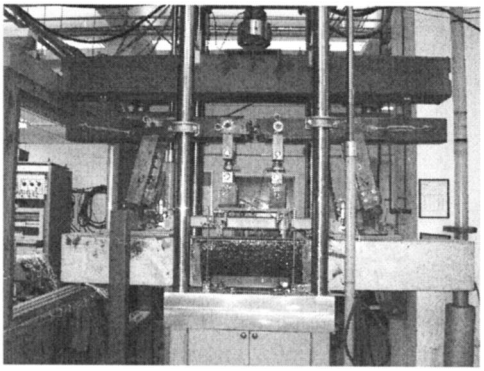

Fig. 6. Fully assembled crosstie and loading rig during test

the pad matched that of the test data up to a pad deflection of 2 mm. This corresponds to an elastic foundation stiffness of 130.8 MPa/m.

Fig. 4 shows the model developed using ten-node tetrahedral solid elements, SOLID 187 (ANSYS 2003). A quarter of the crosstie was modeled to reduce computational effort. All connections were assumed to be perfectly constrained; thus each node connecting different structural members (i.e., brackets, stiffeners, etc.) shared the same degrees of freedom. No uplift of the rail is permitted with this model. The tetrahedral elements were assumed to have an elastic modulus of 200 GPa and a Poisson's ratio of 0.3. The meshing was refined at the connection between the gusset plates and the base plate, the connection between the base plate and the HSS, and the connection between the LIM bracket and the HSS.

Fig. 5 shows the loads that a typical crosstie is subjected to during the passage of a vehicle. An extensive analytical study (Fatemi et al. 1996) and field testing (Campbell et al. 2002) on straight and curved track has shown that the dynamic component of the loading on the crosstie is small for speeds up to 100 km/h. The LIM applies a total force of 19.4 kN upward to the LIM reaction rail. This is transferred to the crosstie through the four LIM reaction rail brackets. The loads on the brackets have been modeled as a uniform pressure load of 0.98 MPa applied on a surface area of 4945 mm^2 on each LIM bracket. Each anchor bolt is pretensioned to 3 kN. In the model, eight point loads of 375 N each were applied uniformly around the edge of each bolt hole. The weight of the vehicle is transferred through the running rails to the base plate. The vehicle weight of 48.4 kN on each side of the crosstie is modeled as a uniform pressure of 1.51 MPa applied to the area directly beneath the running rail: 180 mm (rail width) $\times$178 mm (base plate width). The running rail is banked at a slope of 1/20 (Fig. 2) so that a horizontal load of 13.0 kN is also transferred to the base plate. Previous work (Fatemi et al. 1996; Campbell et al. 2002) indicates that this is an appropriate value for design of the crosstie for fatigue. The horizontal load is modeled by applying horizontal point loads of 433 N to each of the 30 nodes in the area directly beneath the running rail.

Test Program

Fig. 6 shows the custom-designed loading apparatus in the laboratory that simulates the wheel loads from the ART vehicle on the crosstie. Further details on the design of the apparatus are given by Fatemi (1993). The apparatus is mounted and laterally braced within a four-post load frame, and vertical load is applied through an MTS 1,000 kN servo-hydraulic actuator. A load cell at the actuator head continuously monitors the total load and stroke being applied to the apparatus. A load cell is incorporated in each of the two vertical linkages that are used to apply the simulated LIM load between the lower load beams and the crosstie. Spherical bearings between the upper and lower load beams, and pinned joints at all other link connections, ensure statically determinate conditions within the loading apparatus.

A prestressed concrete beam is used as the base of the loading apparatus. The beam was previously drilled and two anchor studs specified for use in the ART track system were chemically anchored into the beam. The studs provide anchor points for the crosstie during the test. The nut on each anchor stud was torqued to 150 N m which results in a preload value of 3.0 kN.

The crosstie was subjected to constant amplitude fatigue loading at a frequency of 1.2 Hz. The minimum vertical applied force was 4 kN to maintain a compressive load on the joints of the test rig and to prevent liftoff in the apparatus from the tie. The maximum vertical force applied to the test apparatus was 77.4 kN.

The fatigue testing was stopped approximately every 100,000 cycles. The rig was loaded quasi-statically up to 77.4 kN and the response recorded. However, a malfunction in the data acquisition equipment prevented data from being recorded for the first 870,000 cycles. Data were collected until a total of 3×10^6 cycles had been applied.

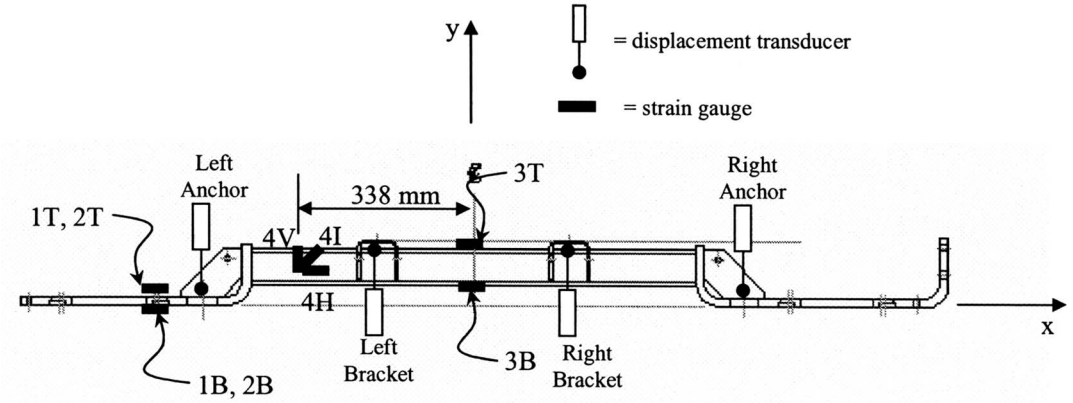

Fig. 7. Location of instrumentation on crosstie

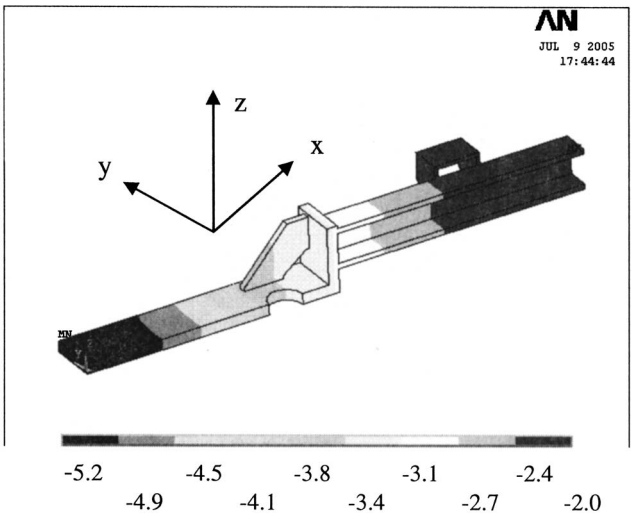

Fig. 8. Predicted vertical deflections of crosstie (units in mm)

Fig. 7 indicates the locations of the four direct current displacement transducers (DCDTs), the six 2 mm linear strain gauges, and the single 45° strain rosette used to monitor crosstie deflections and strains. A critical measure of the performance of the crosstie is the relative deflection between the LIM rail and the running rail. It is impossible to place a displacement transducer directly beneath the running rail. Therefore, displacement transducers were placed as close to the running rail as possible, which was adjacent to the anchor bolts, as shown in Fig. 7.

Change in Air-Gap during Loading

Fig. 8 shows the predicted deflections in the vertical (z direction) when the crosstie is subjected to maximum wheel and LIM loads. All deflections are negative, meaning that the crosstie overall deflects downward. However, the effect of the LIM loads pulling upward on the crosstie results in much smaller deflections at the LIM bracket location and a closing of the air gap.

Fig. 9 compares deflections measured beneath the LIM brackets during static loading, following 3×10^6 cycles of fatigue loading, with the predicted deflections at this location. The load plotted on the ordinate axis is the total vertical load applied by the actuator to the test rig in the case of the test results, or the net vertical load (the wheel loads minus the LIM loads) applied to the

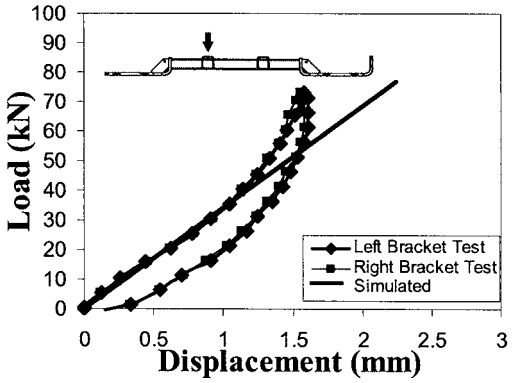

Fig. 9. Comparison of measured and predicted bracket deflections at 3×10^6 cycles

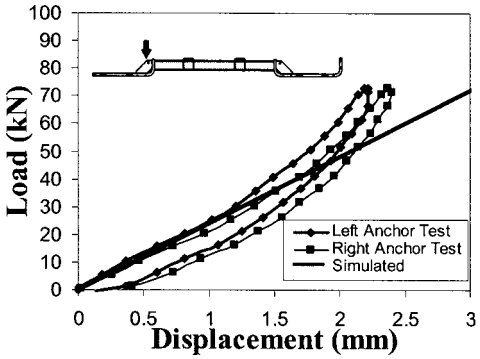

Fig. 10. Comparison of measured and predicted anchor deflections at 3×10^6 cycles

crosstie in the case of the predicted results. The measured load-displacement response during loading is linear up to 40 kN, but gradually becomes stiffer as the load is increased. Hysteresis is evident upon unloading the rig. There is excellent correlation between the measured and predicted displacements up to 40 kN. At higher loads, the predicted displacements are higher than the measured displacements. At the maximum applied load of 77.4 kN, the measured displacement is 1.6 mm, and the predicted displacement is 2.1 mm. Thus, the model conservatively overestimates the bracket displacement at the maximum applied load by 31%. These differences can be attributed to the simplified elastic foundation model used for the elastomeric pad behavior.

Fig. 10 compares deflections measured at the anchor bolt locations during static loading, following 3×10^6 cycles of fatigue loading, with the predicted deflections at this location. Small differences can be noted in the deflections measured at the left anchor and at the right anchor. At the maximum applied load of 77.4 kN, the deflection measured at the left anchor is 2.2 mm, and the deflection measured at the right anchor is 2.4 mm. This is a difference of about 9% and can be attributed to slight misalignments in the loading rig. The measured anchor load-displacement response is essentially linear up to an applied load of 30 kN, after which the response exhibits stiffening. Hysteresis is evident upon unloading the rig. There is good correlation between predicted displacements and the measured left anchor displacements up to 30 kN, and the predicted displacements and the measured right anchor displacements up to 40 kN. At higher loads, the predicted displacements are higher than the measured displacements. At the maximum applied load of 77.4 kN, the measured left anchor displacement is 2.2 mm, and the measured right anchor displacement is 2.4 mm, resulting in an average anchor displacement of 2.3 mm. The predicted displacement is 3.0 mm. Thus, the model conservatively overestimates the average anchor displacement at the maximum applied load by 30%.

Fig. 11 compares measured relative bracket and anchor deflections following 3×10^6 cycles of fatigue loading, with the predicted relative deflections. The relative deflections are the difference between the anchor and LIM bracket deflections at a given load level. Note that this is not a measure of the reduction in the air gap between the LIM primary and the LIM reaction rail, since the air gap reduction is due to the relative deflection between the running rail and LIM bracket. The measured relative deflection response does not show the same degree of stiffening with increasing load noted in the response at the anchor and at the bracket (Figs. 9 and 10). There is little evidence of hysteresis. Considering the nonlinear behavior observed in Figs. 9 and 10,

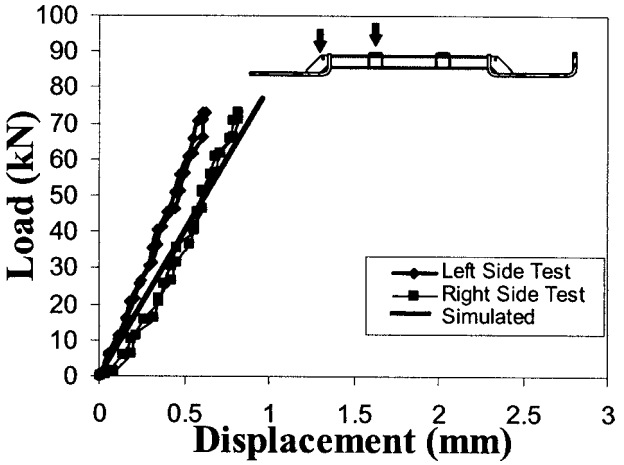

Fig. 11. Comparison of measured and predicted relative deflections at 3×10^6 cycles

the reasons for this are not entirely clear. However, it may suggest that the portion of the deflection measured at the LIM bracket and at the anchor due to deflection of the elastomeric pad is similar. When deflections at the LIM bracket and at the anchor are subtracted to get the relative deflection, the nonlinear deflection due to the elastomeric pad is removed, and only the linear bending of the steel crosstie remains. There are slight differences in the measured relative deflections on the left side of the crosstie and on the right side of the crosstie. At the maximum rig load of 77.4 kN, the left side relative deflection is 0.6 mm and the right side relative deflection is 0.8 mm, giving an average deflection of 0.7 mm. These differences can be related to the misalignment of the crosstie in the loading rig, as noted in the discussion of Fig. 10. There is generally good correlation between the predicted relative deflections and the measured deflections on the right side of the crosstie. The predicted relative deflections are higher than the measured deflections on the left side of the crosstie. At the maximum load, the measured average relative deflection was 0.7 mm, while the predicted relative deflection at this load was 0.9 mm. Thus, the model conservatively overestimates the relative anchor to bracket deflection by 29% at the maximum load on the crosstie.

Fig. 12 shows the maximum relative deflections measured during the loading history of the crosstie. These are relative deflections measured during a static test following the application of a given number of fatigue cycles, and are obtained by averaging the measured relative deflections between the LIM bracket and the anchor for the left and right sides of the crosstie at the maximum load. The relative deflection remained essentially constant at 0.7 mm throughout the load history. This indicates that fatigue cracking, which would cause a change in stiffness and hence a change in deflection, did not occur during the load history. Note that a detailed inspection of the welds of the crosstie would be needed to ensure that microscopic cracking has not been induced during the repeated load test.

The maximum relative deflections actually occur between the running rail and LIM rail, but it is impossible to directly measure these deflections. The FEA model predicts the relative deflection between the bottom of the rail and the top of the LIM bracket to be about 2.0 mm upward. This is a measure of the change in the height of the air gap in the LIM, and larger deflections than this will affect efficient LIM operation. However, based on the comparison of measured and predicted relative deflections, this predicted deflection may overestimate the relative deflection by about 30%.

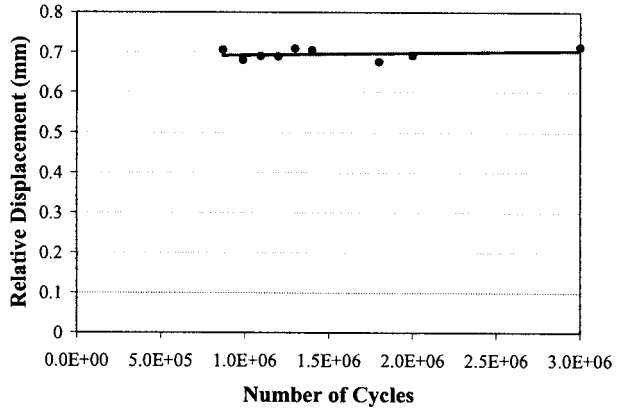

Fig. 12. Relative deflections between LIM and base plate during loading history

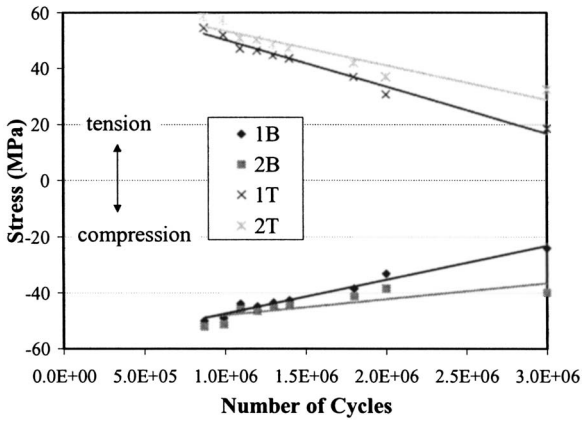

Fig. 13. Stresses in base-plate over loading history

Stresses in Crosstie

Figs. 13 and 14 show stresses in the crosstie determined from the linear strain gauge readings. The strains were converted to stress by multiplying by the assumed elastic modulus for steel,

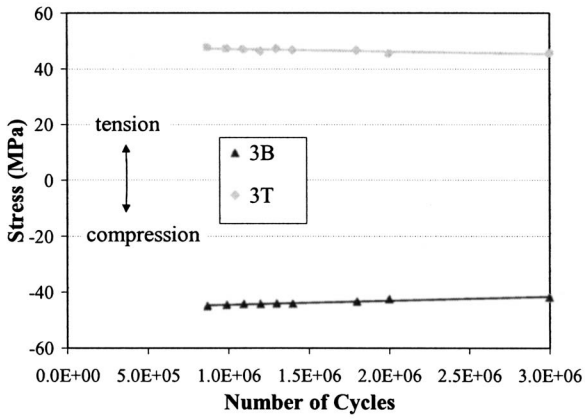

Fig. 14. Stresses in hollow structural section over loading history

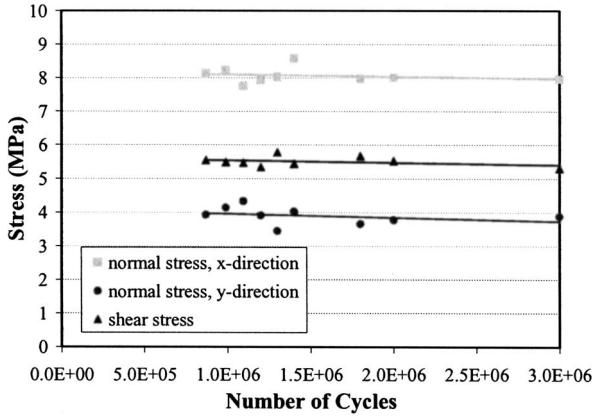

Fig. 15. Stresses at strain rosette locations over loading history

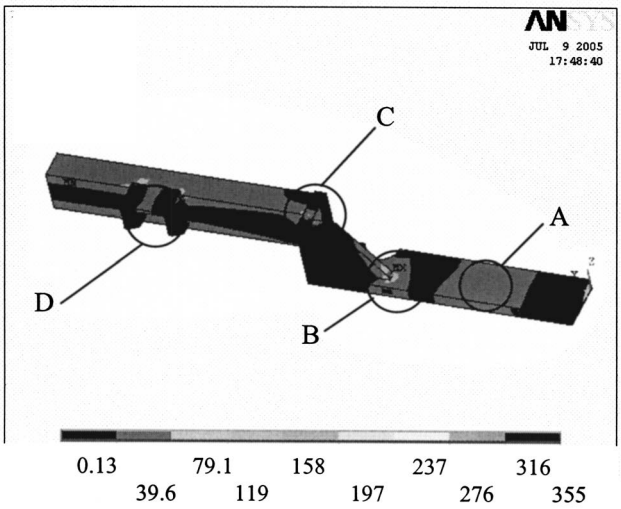

Fig. 16. Predicted von Mises stresses in the crosstie (units in MPa)

$E=200$ GPa. Fig. 14 shows the stress, at an applied load of 77.4 kN, at the top and bottom surfaces of the base plate. Gauges 1T and 2T are mounted on the top surface of the base plate, and Gauges 1B and 2B are mounted on the bottom surface of the base plate (Fig. 7). The magnitude of the stress at the top and bottom of the base plate is virtually the same at each cycle, with the top being in tension and the bottom in compression. This suggests that the base plate at this location is subjected to almost pure bending. Linear trend-line fits to the data in Fig. 13 indicate that the maximum stress decreases with increasing fatigue cycles. At 8.7×10^5 cycles, the stress is 56 MPa in tension at the top and 52 MPa in compression on the bottom. At 3×10^6 cycles, the stress is between 32 and 18 MPa in tension on the top, and between 29 and 40 MPa in compression on the bottom. The reason for the decrease in stress is not clear, but may be due to a cyclic hardening of the steel or relaxation of residual stresses in the gusset plate region. The predicted base-plate stresses at this location from the FEA model were 56.9 MPa in tension and 46.4 MPa in compression for the top and the bottom locations, respectively. These predictions correlate very well with the stresses measured at 8.7×10^5 cycles, with a difference of only 12% for the stresses at the bottom.

Fig. 14 shows the stress at the midspan of the hollow structural section measured at the maximum applied load. The magnitude of the stress at the top (Gauge 3T) and bottom (Gauge 3B) of the section is virtually equal at each load cycle, with the top being in tension and the bottom in compression. Again, this suggests that the hollow structural section is subjected to almost pure bending between the LIM brackets. In contrast to Fig. 13, the trend-line fits to the data in Fig. 14 indicate that the stress between the LIM brackets does not change significantly with increased load cycles, but remains at a constant level of about 47 MPa in tension on top and 42 MPa in compression on the bottom. The FEA model predicts the top and the bottom stresses of the HSS member to be 56.8 MPa in tension and 56.9 MPa in compression, respectively. Thus the model conservatively overestimates the HSS stresses on the top by 21% and on the bottom by 35%.

Fig. 15 shows the maximum stress determined from the strain rosette measurements when the load applied to the crosstie is 77.4 kN. Measured strains were converted to normal stresses in the x and y directions (indicated on Fig. 7) and shear stress using strain transformation equations for a 45° strain rosette and Hooke's law assuming a modulus of steel of $E=200$ GPa and a Poisson's ratio of $\nu=0.3$. The stress condition at the location of the rosette remains relatively constant over the load history of the crosstie. At 3×10^6 cycles, the shear stress is 5.55 MPa when the load applied to the crosstie is 77.4 kN, while the normal stress in the y direction is 3.93 MPa, and in the x direction is 8.13 MPa. An analysis of the strain rosette and load cell results indicated that the apparatus is bending and causing small departures from statically determinate conditions, leading to normal stress in the x direction. The principal stresses for the state of stress at 3×10^6 cycles when the load applied to the crosstie is 77.4 kN are $\sigma_1=11.96$ MPa and $\sigma_2=0.10$ MPa, resulting in a von Mises stress of 11.9 MPa. The model predicts a von Mises stress at the location of the strain rosette to be 13.7 MPa. Therefore, the model conservatively overestimates the stress at this location by 15%.

A comparison of the strain gauge measurements and the finite-element model has confirmed that the model has generally captured the state of stress in the crosstie. The model overestimates the measured stresses by 15–35%. However, the stresses through most of the crosstie are generally small, so the absolute difference in the predicted and measured stresses is in the range of 2–5 MPa.

It is critical that the stresses in the crosstie when subjected to vehicle loads remain below the yield strength of the steel to ensure that permanent deformations do not occur. It is impossible to apply strain gauges at all locations of the crosstie, especially at geometric discontinuities where stress concentrations generally occur. However, the FEA model can be used to estimate the locations and magnitude of the maximum stress in the crosstie. Fig. 16 shows the predicted von Mises stresses in the crosstie under maximum loading. The stresses are generally below 39.6 MPa, which is well below the nominal yield strength of the steel, 350 MPa. Four locations of high stress (A, B, C, D) have been identified in Fig. 16. Table 1 summarizes the maximum stress

Table 1. Maximum Von Mises Stress Predicted by the FEA Model

Label in Fig. 5	Location	Von Mises stress (MPa)[a]
A	Beneath the rail	39.6
B	Toe of gusset-to-base plate connection	89.7
C	Base plate connection	83.2
D	Linear induction motor bracket	41.7

[a]Stresses in the structural members.

predicted at each location. Note that the stresses presented in Fig. 16 are nodal solutions, which means that they are obtained by averaging the stresses from all the elements joined at a given node. This improves the quality of the stress plots but gives incorrect values of the maximum stresses. The values given in Table 1, on the other hand, are the element solutions. The model predicts that the maximum von Mises stress in the base plate will occur at the toe of the gusset-to-base plate connection. High stresses also occur where the HSS connects to the base plate and beneath the running rail. However, the predictions indicate that these local maximum von Mises stresses in the tie are still well below the nominal yield strength of the steel.

Fatigue Performance

The crosstie in service will be subjected to millions of loading cycles, therefore it is critical to ensure that its fatigue performance is adequate. Three million constant amplitude service loads were applied to the crosstie, and no change in stiffness (Fig. 12) or cracking was observed. However, due to time constraints, only a single test was carried out. It is well known that welded components in fatigue can have a wide range of scatter, and the fatigue life at a given stress range can differ by 4.5 times (Savaidis and Vormwald 2000). Therefore, the test results will be compared to fatigue results from other studies of welded components.

The fatigue resistance of welded steel components has traditionally been determined using the classification method. Fatigue test results from welded details of similar configurations are grouped together. For design, the nominal stress determined from beam theory is compared to a stress-life fatigue design curve (van Wingerde et al. 1995). This method is cumbersome, however, when applied to a structure for which the welded details are not similar to conventional details, and the nominal stress is not easily calculated. In the case of the crosstie, conventional fatigue design categories have little data on HSS welded connections. It is also difficult to determine a nominal stress because the crosstie is statically indeterminate and exhibits nonlinear behavior.

The hot spot stress approach has been used successfully as an alternative to the classification method, especially for offshore structures, and has been described in detail by others (van Wingerde et al. 1995). Savaidis and Vormwald (2000) used the hot spot stress approach to evaluate welded connections for the frame structure of an intercity bus.

Fig. 17 shows stresses perpendicular to the welds at locations of high stress in the crosstie. Following the approach of Savaidis and Vormwald (2000), the fillet welds were not modeled explicitly, and the hot spot stress was taken to be the stress that occurs where the weld root would be located. The FEA shows that the highest hot spot stress, 347 MPa, occurs at the corner of the HSS where it is connected to the base plate [Fig. 17(b)].

Savaidis and Vormwald (2000) compared the hot spot stress to the fatigue design curve proposed by the International Institute of Welding (IIW) (Hobbacher 1996). Fig. 18 shows the IIW fatigue design curve. A comparison of the FEA results to the strain gauge measurements suggests that the crosstie stresses can be overestimated by up to 35%. If this were the case, the hot spot stress would be approximately 225 MPa. Fig. 18 also shows the outer range of scatter (10% probability of survival) observed by Savaidis and Vormwald (2000) in their tests of welded connections. The fatigue design curve represents the lower bound of scatter, defined at the 90% probability of survival. The data point obtained from the fatigue testing of the crosstie and the hot spot stress obtained from the FEA, reduced by 35%, is plotted against these results for comparison. It should be noted that the data point is a "run-out" since fatigue cracking was not observed. The experimental data point falls close to, but outside the scatter band. This suggests that the FEA model, even with the reduction of 35%, significantly overestimates the hot spot stress.

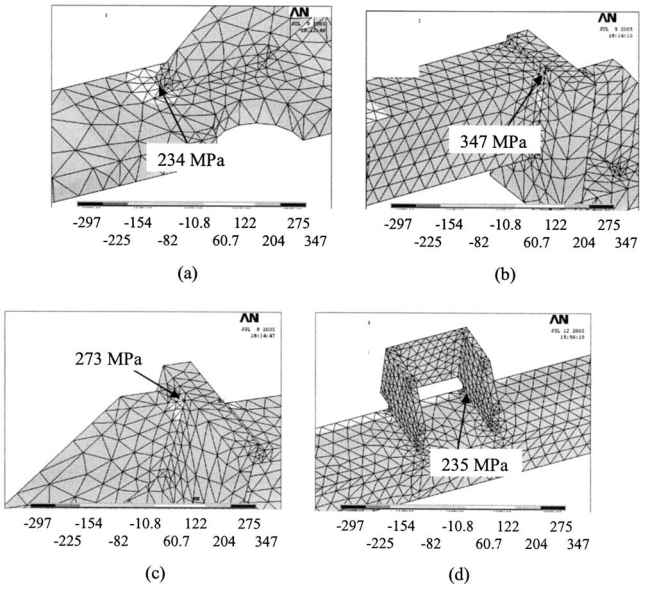

Fig. 17. Maximum normal stress in x direction for welded connections: (a) toe of gusset plate; (b) HSS to baseplate connection; (c) gusset plate to base plate connection; and (d) LIM bracket to HSS connection

Further test results and improved modeling are needed to determine if the hot spot stress approach is a reliable method for determining the fatigue resistance of the crosstie. However, this initial work provides important guidance for further testing and modeling. In particular, the potential locations for fatigue cracking have been clearly identified. The connection between the HSS and the base plate has been identified as the most fatigue critical location. In addition, the results show that the hot spot stress approach will give a conservative prediction of fatigue life for the crosstie.

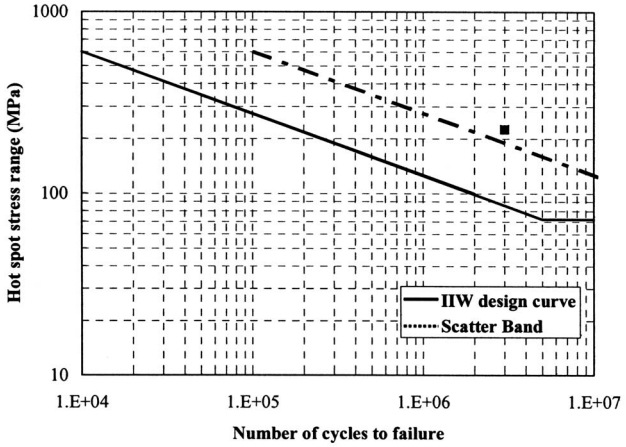

Fig. 18. Fatigue test result and comparison with IIW (Hobbacher 1996) fatigue design curve for use with hot spot stress

Conclusions

A finite-element model of a welded steel crosstie was developed. The model employs tetrahedral elements and elastic foundation elements to represent the elastomeric pad. The model is capable of providing the following:

1. Conservatively predicts deflections during loading of the crosstie to within 30%;
2. Conservatively predicts stresses in the crosstie to within 35%;
3. The fatigue critical location occurs at the HSS to base-plate connection, at the corner of the HSS; and
4. The IIW fatigue design curve and the hot spot stress approach can be used to conservatively assess the crosstie design for constant amplitude fatigue. Further testing and modeling of the crosstie is necessary to reduce the conservatism in using the IIW fatigue curve.

In addition, the experimental work indicates:

1. The crosstie exhibits nonlinear load-deflection response. As the loading increases, the response exhibits stiffening. Upon unloading, the crosstie load-deflection response exhibits hysteresis;
2. The crosstie is capable of sustaining 3×10^6 cycles of service loading with no evidence of macroscopic fatigue cracking;
3. The stresses in the crosstie due to service loading are well below the material yield strength, and no permanent deformation occurs after service loading; and
4. The relative deflections between the LIM rail and base plate of the crosstie are less than the maximum allowable for efficient operation with the vehicle.

Acknowledgments

The contributions of the Total Transit System, Kingston, Ontario, a division of Bombardier Transportation is gratefully acknowledged.

References

ANSYS Inc. (2003). *ANSYS online manual*, Canonsburg, Pa.

Campbell, T. I., Green, M. F., Swanson, D., Moucessian, A., and Skoblenick, H. (2002). "Field testing of an integrated resilient trackwork system." *Proc., 30th Annual Conf. of the Canadian Society for Civil Engineering*, CSCE, Montreal, Paper No. ST-040.

Fatemi, M. J. (1993). "Resilient crosstie track for a transit guide-way." Ph.D. thesis, Queen's Univ., Kingston, Ont., Canada.

Fatemi, M. J., Green, M. F., Campbell, T. I., and Moucessian, A. (1996). "Dynamic analysis of resilient crosstie track for transit system." *J. Transp. Eng.*, 122(2), 173–180.

Hobbacher, A. (1996). "Recommendations for fatigue design of welded joints and components." International Institute of Welding, Document No. XIII-1539-96/XV-845-96, Paris.

Kerr, A. D., and Zarembski, A. M. (1986). "On the new equations for the crosstie track response in the lateral plane." *Rail International*, 17(6), 13–21.

MacDougall, C., Campbell, T. I., Shillinglaw, S., and Skoblenick, H. (2003). "Finite element modeling of an integrated trackwork system." *Proc., 31st Annual Conf. of the Canadian Society for Civil Engineering*, CSCE, Montreal, Paper No. GCF-288.

Savaidis, G., and Vormwald, M. (2000). "Hot-spot stress evaluation of fatigue in welded structural connections supported by finite element analysis." *Int. J. Fatigue*, 22(2), 85–91.

Tarran, F. C. (1987). "Direct measurement of crosstie loads." *Rail International*, 18(1), 37–38.

van Wingerde, A. M., Packer, J. A., and Wardenier, J. (1995). "Criteria for the fatigue assessment of hollow structural section connections." *J. Constr. Steel Res.*, 35(1), 71–115.